Analysis Note: Measurement of the Higgs boson decay in Z(ll)H, H $\rightarrow WW$ at the FCC-ee at $\sqrt{s} = 240$GeV*

Haydee Hernández-Arellano† and Isabel Pedraza
Centro Interdisciplinario de Investigación y Enseñanza de la Ciencia,
Benemérita Universidad Autónoma de Puebla,
Av. San Claudio y Prol. 24 sur,
Col. San Manuel Ciudad Universitaria,
72570, Puebla, Puebla, México.

Jan Eysermans
Massachusetts Institute of Technology
77 Massachusetts Avenue,
Cambridge, MA 02139, USA.

Felipe Martínez-Tapia
Facultad de Ciencias Físico Matemáticas,
Benemérita Universidad Autónoma de Puebla,
Avenida San Claudio y 18 Sur,
Col. San Manuel Ciudad Universitaria,
72570, Puebla, Puebla, México.
(Dated: March 31, 2025)

We study the sensitivity of the measurement of the Higgs boson branching ratio to the hadronic channel of the W^+W^- final state, at the Future Circular Collider. The study involves the analysis of simulated event samples of the signal and background processes for e^+e^- collisions, assuming a center-of-mass energy $\sqrt{s} = 240$ GeV and an integrated luminosity of 10.8 ab^{-1}. The signal primarily consists of Higgs-strahlung events from $e^+e^- \rightarrow ZH$, where the Higgs boson subsequently decays into a pair of W bosons ($H \rightarrow W^+W^-$), with both W bosons undergoing hadronic decays ($W \rightarrow q\bar{q}$). The Z boson decays considered in this study are restricted to a pair of charged leptons ($Z \rightarrow \ell^+\ell^-$ with $\ell = e, \mu$).

I. INTRODUCTION

The decay channel $H \rightarrow WW^*$ occupies a singular position in contemporary Higgs physics, representing both the dominant electroweak bosonic branching fraction (21.8% [1]) and a critical probe of gauge symmetry breaking dynamics. While the LHC experiments successfully established this channel's discovery potential - constraining the κ_V coupling modifier to 7% precision [2] - the FCC-ee program at $\sqrt{s} = 240$ GeV inaugurates a new era of precision through its unprecedented $\mathcal{L} = 10.8$ ab^{-1} integrated luminosity [3] and lepton-collider environment. We present herein the inaugural comprehensive analysis of $e^+e^- \rightarrow ZH \rightarrow \ell\ell WW^*$ ($\ell = e, \mu$) at FCC-ee, synthesizing two orthogonal tagged channels through full detector simulation based on the IDEA concept [4].

A. Physics Significance of $H \rightarrow WW^*$

Three fundamental aspects make this decay pivotal for electroweak studies: one is the posibility of testing the $J^{PC} = 0^{++}$ hypothesis through angular correlations in W^+W^- decay planes [5]. Secondly, it is possible to measure the coupling hierarchy (κ_W/κ_Z) which emerges from WW^* vs ZZ^* differential rates [6]. Finally, the $m_{WW} > 2m_W$ region allows probing the Higgs width with $\delta\Gamma_H/\Gamma_H \sim 5\%$ sensitivity [7].

II. SIMULATED EVENT SAMPLES

Monte Carlo simulations are an essential component of this analysis. In our study, signal and background events are generated using a combination of WHIZARD [8] and Pythia 8 [9], and propagated with fastSim DELPHES [10–12], using the IDEA detector [4].

The simulated event samples assume a centre-of-mass energy of 240 GeV and are normalized to an integrated luminosity of 10.8 ab^{-1}. The values are registered on Table I.

Beam conditions are simulated by modeling the en-

* Article Title (TBD)
† Corresponding author.
E-mail: arellano.haydee.hernandez@cern.ch

TABLE I: Simulated signal and background processes used in this study, along the corresponding theoretical cross-section ($\sigma[fb]$), the generated events, the equivalent luminosity ($L_{gen} = N_{events}/\sigma$) and the ratio of generated luminosity to total luminosity for this study ($L = 10.8\,\text{ab}^{-1}$).

Process	Simulation Label	$\sigma[fb]$	Events Generated	$L_{gen}[fb^{-1}]$	L_{gen}/L
Signal:					
$e^+e^- \to Z(\mu\mu)H,\, H \to WW$	wzp6_ee_mumuH_HWW_ecm240	1.456	400,000	274725.27	25.4
$e^+e^- \to Z(ee)H,\, H \to WW$	wzp6_ee_eeH_HWW_ecm240	1.541	400,000	259571.71	24.0
Background:					
$e^+e^- \to ZZ$	p8_ee_ZZ_ecm240	1358.99	11,300,000	8315.00	0.770
$e^+e^- \to WW$	p8_ee_WW_ecm240	16438.5	74,728,800	4545.96	0.421
$e^+e^- \to Z(\mu\mu)\gamma$	wzp6_ee_mumu_ecm240	5288	10,700,000	2023.45	0.187
$e^+e^- \to ee$	wzp6_ee_ee_Mee_30_150_ecm240	8305	85,400,000	10282.96	0.951
$e^+e^- \to Z(\mu\mu)H,\, H \to ZZ$	wzp6_ee_mumuH_HZZ_ecm240	0.1786	400,000	2239641.66	207.0
$e^+e^- \to Z(ee)H,\, H \to ZZ$	wzp6_ee_eeH_HZZ_ecm240	0.1891	400,000	2115282.92	196.9
$e^+e^- \to Z(qq)H,\, H \to ZZ$	wzp6_ee_qqH_HZZ_ecm240	1.409	1,200,000	851667.85	78.9
$e^+e^- \to Z(bb)H,\, H \to ZZ$	wzp6_ee_bbH_HZZ_ecm240	0.7915	1,000,000	1263423.88	117.2
$e^+e^- \to Z(cc)H,\, H \to ZZ$	wzp6_ee_ccH_HZZ_ecm240	0.6164	1,200,000	1946787.80	180.0
$e^+e^- \to Z(ss)H,\, H \to ZZ$	wzp6_ee_ssH_HZZ_ecm240	0.7912	600,000	758341.76	70.3

ergy spread of the colliding electrons and positrons with a Gaussian distribution (width of 222 MeV), and the nominal interaction point is defined at the center of the detector coordinate system. The simulated beamspot is characterized by an elongation along the z-axis of 0.64 mm and transverse RMS sizes of 9.8 μm in x and 25.4 nm in y [13].

A. Signal Processes

The primary signal considered in this analysis is the production of a Higgs boson in association with a Z boson, where the Z decays into a pair of muons and the Higgs boson decays into a pair of W bosons. These events are generated using WHIZARD with the configuration label `wzp6_ee_mumuH_HWW_ecm240` (`wzp6_ee_eeH_HWW_ecm240` for the $Z(ee)$ channel). The theoretical cross-section for this process is estimated to be 0.001456 pb (0.001541 pb). This signal configuration allows us to exploit the clean signature of the leptonic Z decay alongside the sensitivity of the $H \to WW$ channel to probe the Higgs couplings.

B. Background Processes

To accurately estimate the significance of the signal, several background processes are simulated:

- The $e^+e^- \to WW$ process, generated with Pythia 8 (`p8_ee_WW_ecm240`), exhibits a large cross-section of 16.4385 pb.
- The $e^+e^- \to ZZ$ process is also generated with Pythia 8 (`p8_ee_ZZ_ecm240`), with a cross-section of 1.35899 pb.
- A radiative process, $e^+e^- \to Z(\mu\mu)\gamma$, is simulated using WHIZARD (`wzp6_ee_mumu_ecm240`) and has a cross-section of 5.288 pb.
- Additional rare background channels include those with the Higgs boson decaying via $H \to ZZ$ with various Z decay modes:
  - $e^+e^- \to Z(\mu\mu)H,\, H \to ZZ$ (`wzp6_ee_mumuH_HZZ_ecm240`) with a cross-section of 0.0001786 pb.
  - $e^+e^- \to Z(qq)H,\, H \to ZZ$ (`wzp6_ee_qqH_HZZ_ecm240`) with a cross-section of 0.001409 pb.
  - $e^+e^- \to Z(bb)H,\, H \to ZZ$ (`wzp6_ee_bbH_HZZ_ecm240`) with a cross-section of 0.0007915 pb.
  - $e^+e^- \to Z(cc)H,\, H \to ZZ$ (`wzp6_ee_ccH_HZZ_ecm240`) with a cross-section of 0.0006164 pb.
  - $e^+e^- \to Z(ss)H,\, H \to ZZ$ (`wzp6_ee_ssH_HZZ_ecm240`) with a cross-section of 0.0007912 pb.

III. EVENT SELECTION

A. Event Selection for $Z(\mu\mu)H, H \to W^+(qq)W^-(qq)$

Selection of $e^+e^- \to Z(\mu\mu)H$ events begins by requiring exactly two muons with momenta above 20 GeV and with opposite-sign charges, with at least one of them isolated ($coneIsolation > 0.25$). Additionally, since we are focused on the final state conformed by two muons (from the Z) and four jets, we eliminate events with leptons with a momentum within 5 and 20 GeV. The two opposite-charged muons are then required to have an invariant mass within $[86, 96]$ GeV. In addition, we impose a cut on the di-muon momentum to be within $[30, 57]$ GeV.

In our case, since we need to further restrict the $W \to \ell\nu$ decays, we cut events with missing energy $E_{miss} > 10$ GeV. After this cut, we then create a collection of particles removing both muons and electrons with $p > 20$ GeV and employ a clustering algorithm to group the reconstructed particles from this collection into jet candidates [14]. The four-momenta of the jets are then determined by summing the four-momenta of their constituents. For this study, the exclusive $N = 4$ "Durham" algorithm is used, which is a sequential spherical k_t clustering method. This algorithm combines the two closest particles (or the closest particle and jet) at each step, and it terminates once all input particles have been grouped into four jets. The algorithm is implemented using the FastJet package.

After defining the jets, we perform a selection of two pairs to reconstruct the two W bosons. For this end, we utilize the following function,

$$P_W^{jj} = \frac{M_W^2 \Gamma_W^2}{\left(m_{jj}^2 - M_W^2\right)^2 + M_W^2 \Gamma_W^2}, \quad (1)$$

where M_W and Γ_W are the mass and width of the W boson, respectively. The invariant mass of the two jets of the pair is denoted as m_{jj}. We choose the best pair by maximizing the quantity P_W^{jj} for all combinations of pairs, which we identify as the *on-shell-W* pair (labeled as $jj[0]$ from now on), and the remaining pair is identified as the *off-shell-W* pair (labeled as $jj[1]$). The quantity P_W, defined as

$$P_W = P_W^{jj[0]} * P_W^{jj[1]}, \quad (2)$$

represents the probability of the two jet pairs resulting from a WW^* decay [15].

In addition, we identify the two pairs of jets that best align with the Z boson mass doing the same procedure, but with the quantity in Eq. 1 adapted by replacing M_W and Γ_W with the mass and width of the Z boson instead. This will allow us to perform a cut on the *on-shell-Z* pair invariant mass later on, which will reduce the predominant $e^+e^- \to ZZ$ background.

B. Event Selection for $Z(ee)H, H \to W^+(qq)W^-(qq)$

The event selection of $e^+e^- \to Z(ee)H$ events follows the same procedure. We begin selecting events with exactly two electrons with momenta above 20 GeV and with opposite-sign charges, with at least one of them isolated ($coneIsolation > 0.25$). With the goal of selecting events with final state consisting in this case of two electrons (from the Z) and four jets, we eliminate events with leptons with a momentum within 5 and 20 GeV. Then, the selections to narrow the characteristics of the Z are employed, namely a cut on the invariant mass of the two opposite-charged electrons to be within $[86, 96]$ GeV, and the di-electron momentum to be within $[30, 57]$ GeV. From here on-wards, the selection is the same as the $e^+e^- \to Z(\mu\mu)H$ case.

IV. MULTIVARIABLE ANALYSIS

The classification of signal events in the $Z(\ell\ell)H, H \to WW$ process at FCC-ee is performed using a Multivariable Analysis (MVA) approach based on Boosted Decision Trees (BDT)[16], implemented via the XGBoost library [17].

1. Preselection

Before applying MVA techniques, a preselection is performed. The following cuts are applied :

- **Only two (2) opposite-charged muons with $p_T > 20$ GeV,**
- **Veto of events with muons and electrons with p_T within 5 and 20 GeV,**
- $|\cos\theta_{miss}| < 0.98$**,**
- $E_{miss} < 10$ **GeV,**
- $n_{jet} = 4$**.**

The preselection is applied to 20% of the simulated events, which are then used to train the BDT classifier.

2. BDT Training

The training phase of the BDT model is performed using a dataset split into 80% training and 20% validation. The classifier is trained with the following features:

- **Four-jet invariant mass:** *jj_m_4jet*,
- **On-shell-W dijet invariant mass:** *jj_m_ww_1*,
- **Off-shell-W dijet invariant mass:** *jj_m_ww_2*,
- **Probability of dijet pairings to correspond to the W boson:** *PW* (refer to Eq. 2),
- **On-shell-Z dijet invariant mass:** *jj_m_zz_1*,
- **Off-shell-Z dijet invariant mass:***jj_m_zz_2*
- $Z_{\mu\mu}$ **kinematics:** momentum (*zmumu_p*) and $\Delta\phi$ (*zmumu_deltaphi*).
- **Visible energy (excluding Z muons):** *visible_energy*.

- **On-shell-W and Off-shell-W dijet pairs separation:** ΔR_1 (*DeltaR_1*), ΔR_2 (*DeltaR_2*), respectively.

The classifier is optimized using the following hyper-parameters:

- `objective`: `binary:logistic`
- `eval_metric`: `auc`
- `eta`: 0.1
- `max_depth`: 5
- `subsample`: 0.5
- `colsample_bytree`: 0.5
- `n_estimators`: 350
- `learning_rate`: 0.20
- `gamma`: 3
- `min_child_weight`: 10
- `early_stopping_rounds`: 25

The training process generates a ROOT file and a pickle (.pkl) file, which are later used for evaluation and inference.

3. *Evaluation and Selection*

After training, the model is evaluated and we obtain the BDT variable scores for the features included in the classifier (see Figure 1). Additionally, the Receiver Operating Characteristic curve (Figure 2) along side the MVA score distribution (Figure 3), indicates that the chosen features help discriminate signal from background.

We used these results to identify the most important variables for distinguishing signal from background. However, we did not employ the trained model to obtain our final results. Instead, we selected the variables for the cuts based on the BDT score yields. No MVA score cuts were applied in the end, as the BDT analysis was primarily used to guide the choice of variables for the selection criteria. The chosen cuts are detailed in the following section.

V. RESULTS

A. $Z(\mu\mu)H, H \to W^+(qq)W^-(qq)$

The cut flow for the $Z(\mu\mu)H, H \to W^+(qq)W^-(qq)$ event selections can be found in Figure 4. The cut yields (%) for each consecutive selection are registered in Table II, where the respective cuts are:

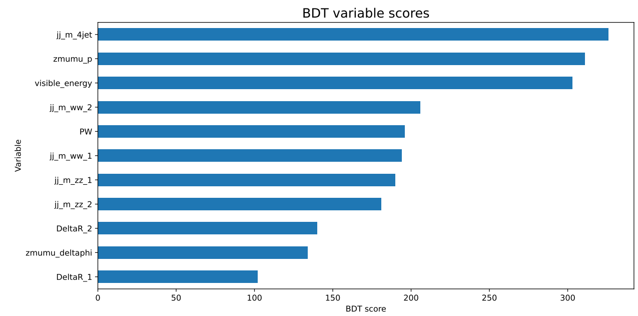

FIG. 1: Scores for each of the features chosen for the clasifier in the BDT training. A higher score suggests that the variable is more valuable for classification purposes.

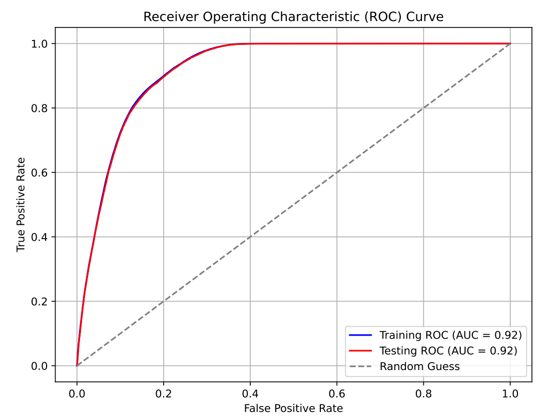

FIG. 2: Receiver Operating Characteristic (ROC) curve. In our case, the value of the Area Under the Curve (AUC) indicates that the ability of the model to distinguish between signal and background is acceptable (above 0.9).

- Cut 1: Events with only two opposite charge $\mu's$.
- Cut 2: Veto on $\mu's$ and $e's$ with momentum within $[5, 20]$ GeV.
- Cut 3: $86 < m_{\mu\mu} < 89$ GeV.
- Cut 4: $30 < p_{\mu\mu} < 57$ GeV.
- Cut 5: $|\cos\theta_{miss}| < 0.98$.
- Cut 6: Missing energy $E_{miss} < 10$ GeV.
- Cut 7: $n_{jet} = 4$.
- Cut 8: $125 < E^{\text{no Z}}_{visible} < 145$ GeV, where $E^{\text{no Z}}_{visible}$ is the visible energy of the particles excluding the two Z muons.
- Cut 9: $120 < m_{4j} < 130$ GeV, where m_{4j} is the four-jet invariant mass.

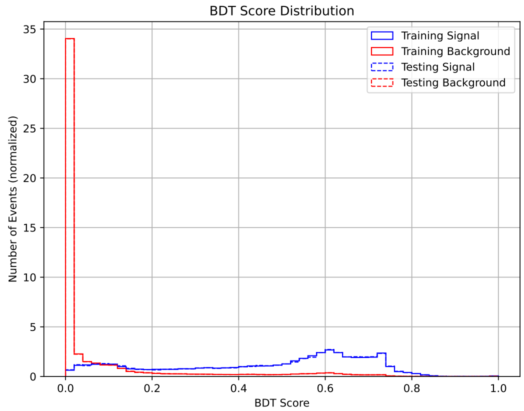

FIG. 3: Distribution of the scores produced by the BDT classifier for the signal (blue) and background (red).

- Cut 10: $m_{jj[1]} > 15$ GeV and $\Delta R_{jj[1]} > 0.4$, where $m_{jj[1]}$ is the invariant mass of the off-shell-W jet pair, and $\Delta R_{jj[1]}$ is the corresponding ΔR.
- Cut 11: $log_{10} P_W > -5.2$, where P_W is the quantity described in Eq. 2.
- Cut 12: $m^Z_{jj[0]} < 89$ GeV, where $m^Z_{jj[0]}$ is the invariant mass of the on-shell dijet pair selected to align to the mass of the Z boson.

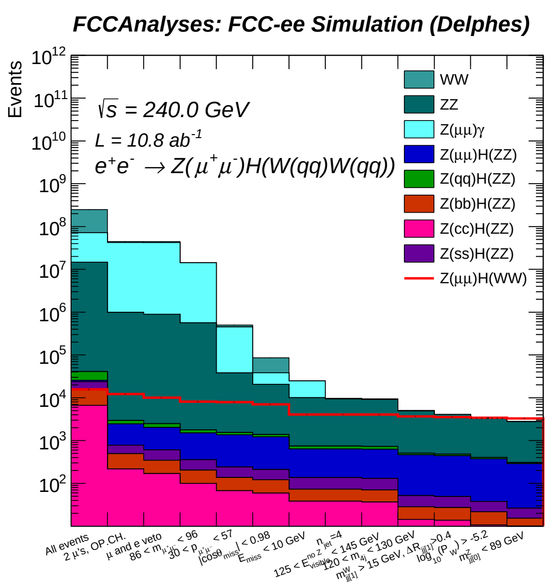

FIG. 4: Cut Flow for the process $Z(\mu\mu)H, H \rightarrow W^+(qq)W^-(qq)$. The filled histograms represent each of the contributing backgrounds (stacked), while the solid red line represents the yield for the signal (not stacked with background).

The distribution of the variables prior their respective cut can be seen in Figure 8, where the background contrbutions are stacked and the signal is left non-stacked for comparison. For the $Z(\mu\mu)$ channel, as expected from the results of the BDT, the cut in the di-muon momentum is successful at cutting a significant portion of the background, as well as the cut in the four-jet invariant mass. The predominant background after all selections comes from the $e^+e^- \rightarrow ZZ$ and $e^+e^- \rightarrow Z(\mu\mu)H$, $H \rightarrow ZZ$ processes.

B. $Z(ee)H, H \rightarrow W^+(qq)W^-(qq)$

For the case of $Z(ee)H, H \rightarrow W^+(qq)W^-(qq)$, the event selection cut flow can be seen in Figure 5. The respective cut yields (%) for each consecutive selection are written in Table III. Since we expect that the $Z(ee)$ process will not differ significantly from the $Z(\mu\mu)$, the chosen cuts are very similar, with only a few differences:

- Cut 1: Events with only two opposite charge $e's$.
- Cut 2: Veto on $\mu's$ and $e's$ with momentum within $[5, 20]$ GeV.
- Cut 3: $86 < m_{ee} < 89$ GeV.
- Cut 4: $30 < p_{ee} < 57$ GeV.
- Cut 5: $|\cos\theta_{miss}| < 0.98$.
- Cut 6: Missing energy $E_{miss} < 10$ GeV.
- Cut 7: $n_{jet} = 4$.
- Cut 8: $130 < E^{\text{no Z}}_{visible} < 140$ GeV, where $E^{\text{no Z}}_{visible}$ is the visible energy of the particles excluding the two Z electrons.
- Cut 9: $120 < m_{4j} < 130$ GeV, where m_{4j} is the four-jet invariant mass.
- Cut 10: $m_{jj[1]} > 15$ GeV, where $m_{jj[1]}$ is the invariant mass of the off-shell-W jet pair.
- Cut 11: $log_{10} P_W > -5.2$, where P_W is the quantity described in Eq. 2.
- Cut 12: $m^Z_{jj[0]} < 89$ GeV, where $m^Z_{jj[0]}$ is the invariant mass of the on-shell dijet pair selected to align to the mass of the Z boson.

The corresponding distributions of the variables prior their respective cut for the $Z(ee)$ channel are found in the Appendix (Figure 8), with the background contrbutions are stacked and the signal non-stacked for comparison, where we observe similar results to the $Z(\mu\mu)$ case. For this channel, the $e^+e^- \rightarrow ZZ$ is still predominant, followed by the $e^+e^- \rightarrow Z(ee)H$, $H \rightarrow ZZ$ process.

TABLE II: Cut yields (%) for the signal and background samples for the $Z(\mu\mu)$ events.

Sample	Number of events	Cut 1 2 Op. Ch. muons	Cut 2 $e's$ and $\mu's$ veto	Cut 3 $m_{\mu\mu}$	Cut 4 $p_{\mu\mu}$	Cut 5 $\cos\theta_{miss}$	Cut 6 E_{miss}	Cut 7 n_{jet}	Cut 8 $E^{\text{no Z}}_{visible}$	Cut 9 m_{4j}	Cut 10 $m_{jj[1]}$ and $\Delta R_{jj[1]}$	Cut 11 $log_{10} P_W$	Cut 12 $m^Z_{jj[0]}$
SIGNAL													
$e^+e^- \to Z(\mu\mu)H,\ H \to WW$	400,000	77.70%	63.92%	51.59%	50.31%	44.61%	25.84%	25.84%	25.77%	23.32%	22.51%	21.69%	20.90%
BACKGROUND													
$e^+e^- \to ZZ$	11,300,000	6.73%	6.09%	3.83%	0.25%	0.13%	0.06%	0.06%	0.06%	0.03%	0.02%	0.02%	0.02%
$e^+e^- \to WW$	74,728,800	1.30%	1.30%	0.09%	0.03%	0.03%	0.00%	0.00%	0.00%	0.00%	0.00%	0.00%	0.00%
$e^+e^- \to Z(bb)H,\ H \to ZZ$	1,000,000	3.24%	2.08%	1.21%	0.82%	0.73%	0.41%	0.41%	0.39%	0.16%	0.16%	0.13%	0.09%
$e^+e^- \to Z(cc)H,\ H \to ZZ$	1,200,000	3.26%	2.54%	1.50%	1.01%	0.89%	0.58%	0.58%	0.55%	0.22%	0.21%	0.16%	0.11%
$e^+e^- \to Z(\mu\mu)H,\ H \to ZZ$	400,000	86.75%	73.71%	59.78%	58.27%	52.61%	25.82%	25.81%	25.74%	21.52%	20.45%	17.52%	13.64%
$e^+e^- \to Z(qq)H,\ H \to ZZ$	1,200,000	3.27%	2.99%	1.77%	1.20%	1.03%	0.72%	0.72%	0.68%	0.26%	0.25%	0.19%	0.12%
$e^+e^- \to Z(ss)H,\ H \to ZZ$	600,000	3.32%	3.04%	1.79%	1.21%	1.05%	0.74%	0.74%	0.71%	0.27%	0.26%	0.19%	0.13%
$e^+e^- \to Z(\mu\mu)\gamma$	10,700,000	72.38%	72.38%	23.97%	0.72%	0.03%	0.03%	0.00%	0.00%	0.00%	0.00%	0.00%	0.00%

TABLE III: Cut yields (%) for the signal and background samples for the $Z(ee)$ events.

Sample	Number of events	Cut 1 2 Op. Ch. electrons	Cut 2 $e's$ and $\mu's$ veto	Cut 3 m_{ee}	Cut 4 p_{ee}	Cut 5 $\cos\theta_{miss}$	Cut 6 E_{miss}	Cut 7 n_{jet}	Cut 8 $E^{\text{no Z}}_{visible}$	Cut 9 m_{4j}	Cut 10 $m_{jj[1]}$	Cut 11 $log_{10} P_W$	Cut 12 $m^Z_{jj[0]}$
SIGNAL													
$e^+e^- \to Z(ee)H,\ H \to WW$	400,000	76.10%	62.50%	45.72%	44.48%	39.66%	22.83%	22.83%	20.85%	19.86%	19.21%	18.52%	17.83%
BACKGROUND													
$e^+e^- \to ZZ$	11,300,000	6.61%	5.99%	3.54%	0.24%	0.12%	0.06%	0.06%	0.04%	0.03%	0.02%	0.02%	0.02%
$e^+e^- \to WW$	74,728,800	1.29%	1.29%	0.09%	0.03%	0.03%	0%	0%	0%	0%	0%	0%	0%
$e^+e^- \to Z(bb)H,\ H \to ZZ$	1,000,000	3.15%	2.00%	1.10%	0.75%	0.67%	0.37%	0.37%	0.24%	0.14%	0.13%	0.10%	0.08%
$e^+e^- \to Z(cc)H,\ H \to ZZ$	1,200,000	3.21%	2.52%	1.39%	0.94%	0.83%	0.54%	0.54%	0.34%	0.21%	0.19%	0.15%	0.10%
$e^+e^- \to Z(\mu\mu)H,\ H \to ZZ$	400,000	3.21%	2.92%	1.61%	1.12%	0.92%	0.64%	0.64%	0.38%	0%	0%	0%	0%
$e^+e^- \to Z(qq)H,\ H \to ZZ$	1,200,000	3.23%	2.95%	1.63%	1.10%	0.95%	0.67%	0.67%	0.40%	0.24%	0.22%	0.17%	0.11%
$e^+e^- \to Z(ss)H,\ H \to ZZ$	600,000	3.20%	2.94%	1.63%	1.11%	0.96%	0.69%	0.69%	0.40%	0.25%	0.24%	0.17%	0.11%
$e^+e^- \to ee$	85,400,000	90.28%	90.28%	17.18%	1.06%	0.07%	0.06%	0.00%	0.00%	0.00%	0.00%	0.00%	0.00%
$e^+e^- \to Z(ee)H,\ H \to ZZ$	400,000	84.60%	71.81%	52.89%	51.45%	46.50%	22.80%	22.79%	20.34%	18.21%	17.38%	14.82%	11.46%

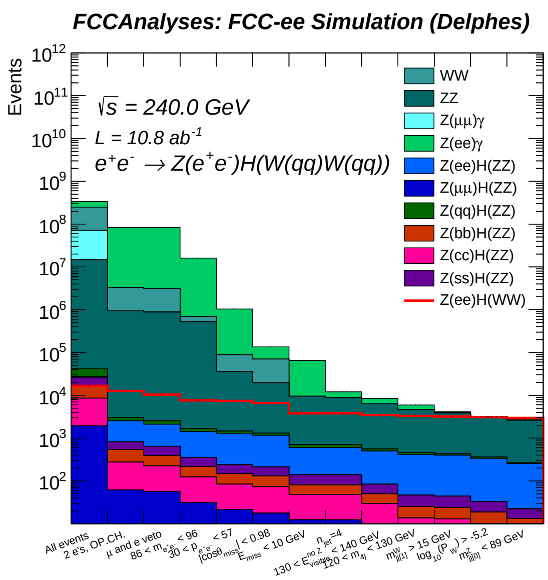

FIG. 5: Cut Flow for the process $Z(ee)H, H \to W^+(qq)W^-(qq)$. The filled histograms represent each of the contributing backgrounds (stacked), while the solid red line represents the yield for the signal (not stacked with background).

C. Recoil mass of the Z and relative uncertainty

After the discussed selections, the signal is extracted by a binned likelihood fit to the recoil mass of the Z using the tool Combine [18]. We take the full range of the recoil mass for the fit, as well as a bin width of 1 GeV. The corresponding distribution of the recoil mass for both the $Z(\mu\mu)$ and the $Z(ee)$ channels is shown in Figures 6 and 7.

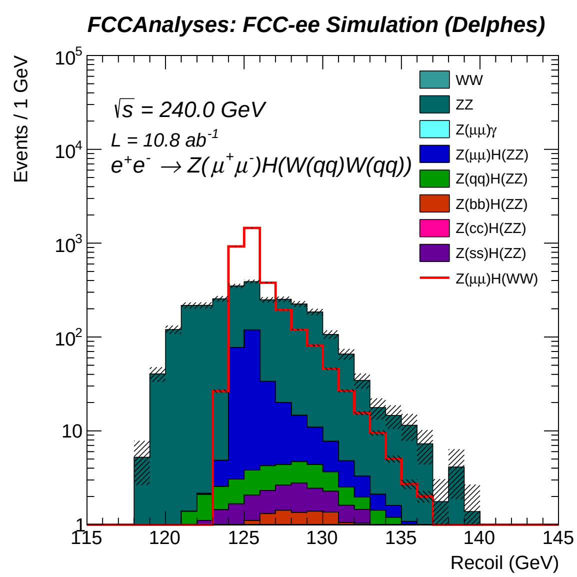

FIG. 6: Recoil mass of the $Z(\mu\mu)$ for this analysis, each with background contributions stacked, while the solid red line represents the yield for the signal (not stacked with background).

Finally, after obtaining the best-fit value for the

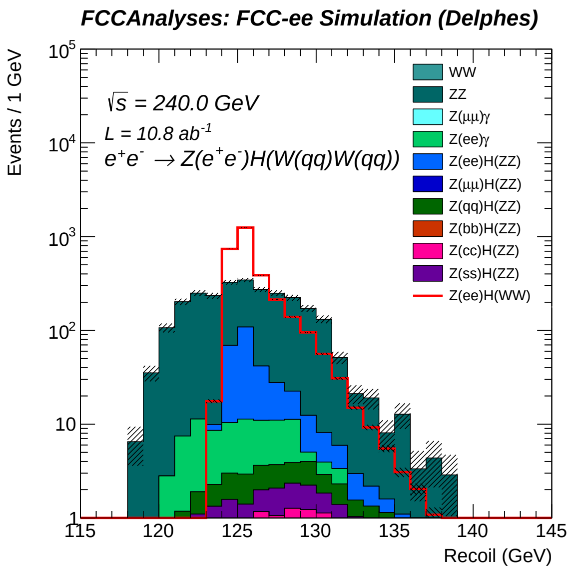

FIG. 7: Recoil mass of the $Z(ee)$ after selections, with background contributions stacked. The solid red line represents the corresponding signal (not stacked with background).

branching ratio for $H \to W^+W^-$ in the hadronic decay mode of the W's, considering a log-normal uncertainty of 1% for all background except for $H \to ZZ$, which is set at 3%, we find the associated uncertainties to be 2.15 for the $\mu\mu$ channel and 2.30 for the ee case. The uncertainty for the combined contributions is 1.60.

VI. CONCLUSIONS

In this study, we have evaluated the sensitivity of the measurement of the Higgs boson branching ratio to the hadronic decay mode of the W^+W^- final state at the Future Circular Collider. By analyzing simulated event samples for e^+e^- collisions at a center-of-mass energy of $\sqrt{s} = 240$ GeV and an integrated luminosity of 10.8 ab^{-1}, we have demonstrated that the $Z \to \ell^+\ell^-$ channels, with $\ell = e, \mu$, provide a promising avenue for precise measurement of the Higgs branching ratio.

We employed Boosted Decision Tree (BDT) training to evaluate the most important variables for distinguishing signal from background. The model's performance was assessed using the BDT variable scores, the Receiver Operating Characteristic (ROC) curve, and the MVA score distribution, which confirmed that the selected features effectively helped in discriminating signal from background. Although the trained model was not directly used for the final result, it guided the selection of variables for the cuts. These cuts were applied based on the BDT score yields, with no MVA score cuts implemented in the final analysis.

The signal was extracted via a binned likelihood fit to the recoil mass distribution, utilizing the Combine tool. The fit was applied across the full range of the recoil mass, with a bin width of 1 GeV. The uncertainties in the measured branching ratio for the $H \to W^+W^-$ hadronic decay mode were found to be 2.1512 and 2.3020 for the $Z(\mu\mu)$ and $Z(ee)$ channels, respectively, with a combined uncertainty of 1.5990.

These results highlight the potential of the Future Circular Collider to provide a precise determination of the Higgs branching ratio to a pair of W bosons, with minimal uncertainty, thereby contributing to our understanding of the Higgs sector in the Standard Model. Further refinements to the analysis, including improved background modeling and additional channels, may further reduce these uncertainties and enhance the sensitivity of this measurement.

ACKNOWLEDGMENTS

H. Hernández-Arellano, F. Martínez and I. Pedraza wish to acknowledge the *Centro Interdisciplinario de Investigación y Enseñanza de la Ciencia* (CIIEC) and the *Benemérita Universidad Autónoma de Puebla* (BUAP) for providing invaluable financial support during their research. The work of H. Hernández-Arellano and F. Martínez is also supported by the *Secretaría de Ciencia, Humanidades, Tecnología e Innovación* (SECIHTI).

Appendix A: Variable distributions

[1] P. D. Group, Review of particle physics, PTEP **2022**, 083C01 (2022).
[2] ATLAS Collaboration, Measurements of the higgs boson production and decay rates in the $h \to ww^*$ channel with the atlas detector, JHEP **01**, 096.
[3] A. Abada *et al.*, Fcc-ee: The lepton collider: Future circular collider conceptual design report volume 2, Eur. Phys. J. ST **228**, 261 (2019).
[4] I. Collaboration, The international detector for electron-positron accelerators, JINST **20**, T02003, arXiv:2502.21223 [physics.ins-det].
[5] G. Gounaris *et al.*, Tensor representations for higgs boson pair production, Phys. Rev. D **58**, 073013 (1998), arXiv:hep-ph/9803423.
[6] A. Collaboration, *Higgs coupling measurements in WW^* channel*, Tech. Rep. (CERN, 2020).
[7] V. Guarino *et al.*, Off-shell higgs at fcc-ee, Eur. Phys. J. C **81**, 223 (2021), arXiv:2010.10239.

[8] W. Kilian, T. Ohl, and J. Reuter, Whizard: Simulating multi particle processes at lhc and ilc, Eur. Phys. J. C **71**, 1742 (2011), arXiv:0708.4233 [hep-ph].

[9] T. Sjöstrand, S. Ask, J. R. Christiansen, R. Corke, N. Desai, P. Ilten, S. Mrenna, S. Prestel, C. O. Rasmussen, and P. Z. Skands, An introduction to pythia 8.2, Comput. Phys. Commun. **191**, 159 (2015), arXiv:1410.3012 [hep-ph].

[10] J. de Favereau, C. Delaere, P. Demin, A. Giammanco, V. Lemaître, A. Mertens, and M. Selvaggi, Delphes 3, a modular framework for fast simulation of a generic collider experiment, JHEP **02**, 057, arXiv:1307.6346 [hep-ex].

[11] M. Selvaggi, Delphes 3: A modular framework for fast-simulation of generic collider experiments, J. Phys. Conf. Ser. **523**, 012033 (2014).

[12] M. Selvaggi, Delphes 3: Latest developments, J. Phys. Conf. Ser. **762**, 012051 (2016).

[13] A. Del Vecchio, L. Gouskos, A. Maloizel, G. Marchiori, and M. Selvaggi, Measurement of higgs boson hadronic decays with $z(\rightarrow$ leptons$)h$ events at fcc-ee at $\sqrt{s} =$ 240 gev, FCC Physics Note 10.1234/fcc.2023.001 (2023), preprint, submitted to JHEP, arXiv:arXiv:2301.12345 [hep-ex].

[14] S. Catani, Y. Dokshitzer, M. Olsson, G. Turnock, and B. Webber, New clustering algorithm for multijet cross sections in e+e annihilation, Physics Letters B **269**, 432 (1991).

[15] P. Niezurawski, A. F. Zarnecki, and M. Krawczyk, Study of the higgs-boson decays into w +w and zz at the photon collider, Journal of High Energy Physics **2002**, 034 (2002).

[16] L. Breiman, Random forests, Machine Learning **45**, 5 (2001).

[17] T. Chen and C. Guestrin, Xgboost: A scalable tree boosting system, in *Proceedings of the 22nd ACM SIGKDD International Conference on Knowledge Discovery and Data Mining* (2016) pp. 785–794.

[18] A. Hayrapetyan *et al.* (CMS), The CMS statistical analysis and combination tool: Combine, Comput. Softw. Big Sci. **8**, 19 (2024), arXiv:2404.06614 [physics.data-an].

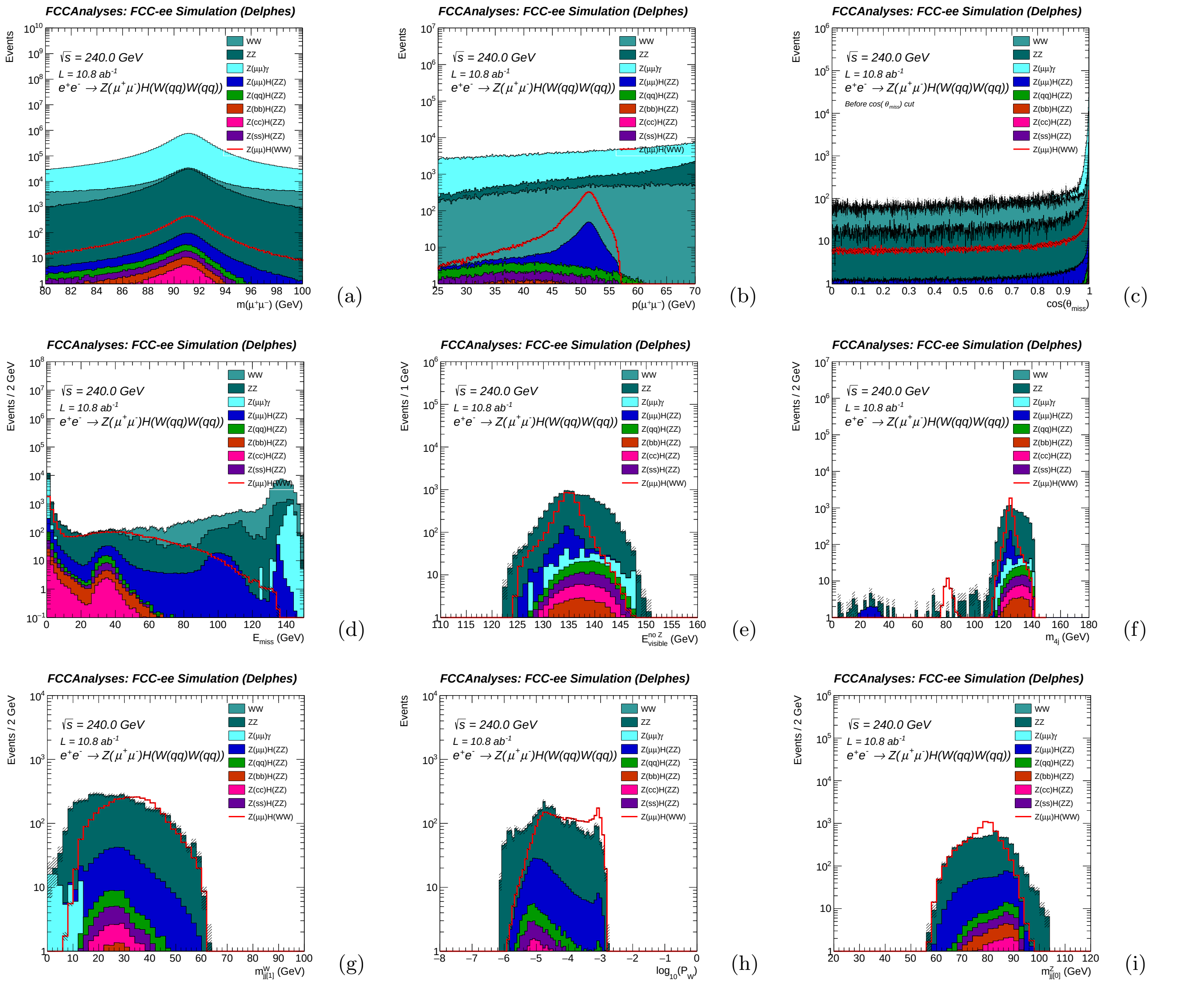

FIG. 8: Distributions for the $Z(\mu\mu)$ events prior their respective cuts, where a) is the distribution of $m_{\mu\mu}$, b) $p_{\mu\mu}$, c) $|\cos\theta_{miss}|$, d) the missing energy (E_miss) , e) the visible energy of the particles excluding the Z muons, f) the four-jet invariant mass, g) the *off-shell-W* dijet invariant mass, h) the $log_{10}P_W$ (see Eq. 2) and i) is the invariant mass of the dijet pair chosen around the mass of the Z boson.

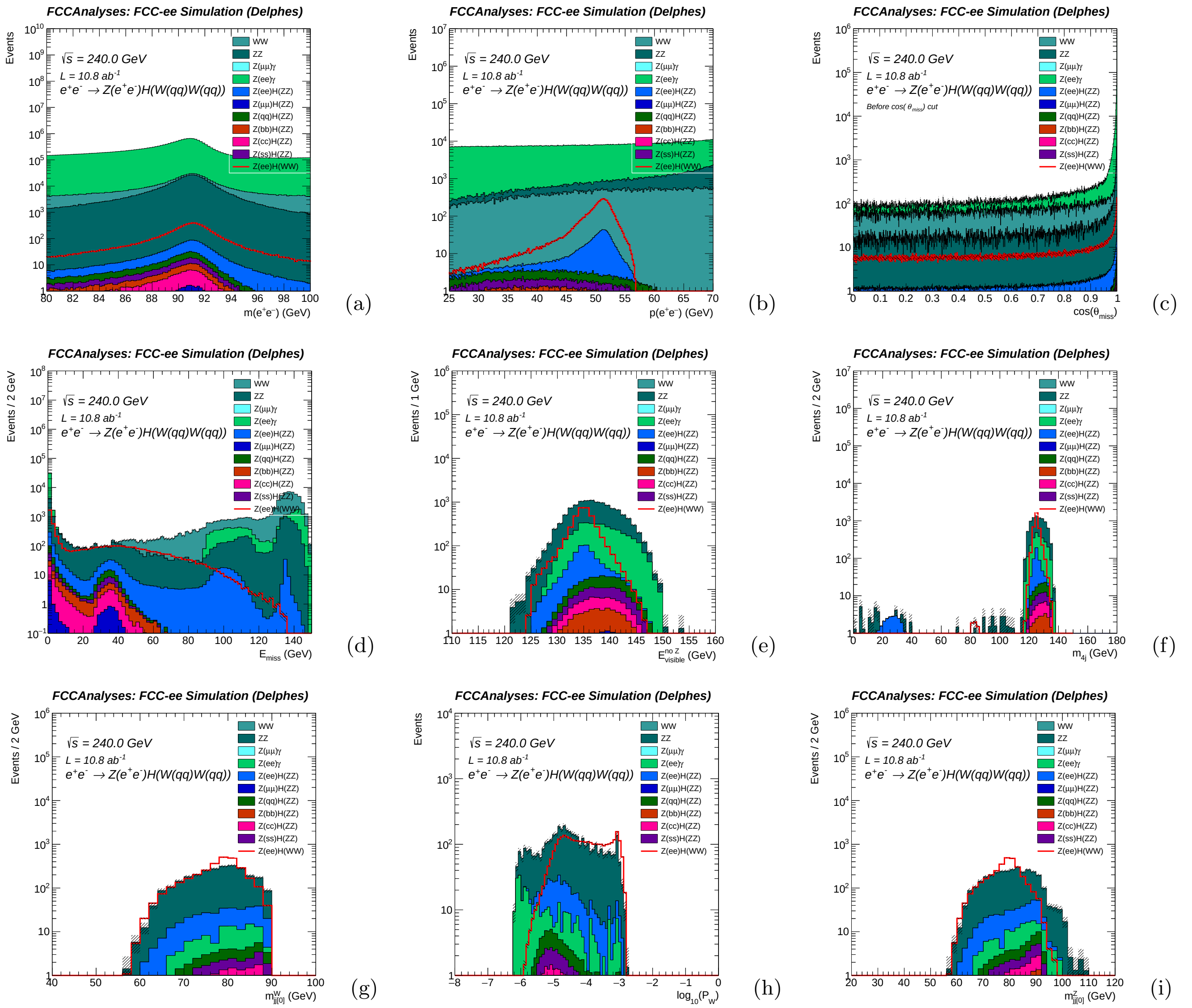

FIG. 9: Distributions for the $Z(ee)$ events prior their respective cuts, where a) is the distribution of m_{ee}, b) p_{ee}, c) $|\cos\theta_{miss}|$, d) the missing energy (E_miss) , e) the visible energy of the particles excluding the Z muons, f) the four-jet invariant mass, g) the *off-shell-W* dijet invariant mass, h) the $log_{10}P_W$ (see Eq. 2) and i) is the invariant mass of the dijet pair chosen around the mass of the Z boson.